Contents lists available at ScienceDirect

Nuclear Engineering and Technology

journal homepage: www.elsevier.com/locate/net

Original Article

Time dependent heat transfer of proliferation resistant plutonium

Cody Lloyd[*], Ravi Hadimani, Braden Goddard

Virginia Commonwealth University, Department of Mechanical and Nuclear Engineering, 401 West Main Street, P.O. Box 843015, Richmond, VA, 23284-3015, USA

A B S T R A C T

Increasing proliferation resistance of plutonium by way of increased ^{238}Pu content is of interest to the nuclear nonproliferation and international safeguards community. Considering the high alpha decay heat of ^{238}Pu, increasing the isotopic fraction leads to a noticeably higher amount of heat generation within the plutonium. High heat generation is especially unattractive in the scenario of weaponization. Upon weaponization of the plutonium, the plutonium may generate enough heat to elevate the temperature in the high explosives to above its self-explosion temperature, rendering the weapon useless. In addition, elevated temperatures will cause thermal expansion in the components of a nuclear explosive device that may produce thermal stresses high enough to produce failure in the materials, reducing the effectiveness of the weapon. Understanding the technical limit of ^{238}Pu required to reduce the possibility of weaponization is key to reducing the current limit on safeguarded plutonium (greater than 80 at. % ^{238}Pu). The plutonium vector evaluated in this study was found by simulating public information on Lightbridge's fuel design for pressurized water reactors. This study explores the temperature profile and maximum stress within a simple (first generation design) hypothetical nuclear explosive device of four unique scenarios over time. Analyzing the transient development of both the temperature profile and maximum stress not only establishes a technical limit on the ^{238}Pu content, but also establishes a time limit for which each scenario would be useable.

© 2018 Korean Nuclear Society, Published by Elsevier Korea LLC. This is an open access article under the CC BY-NC-ND license (http://creativecommons.org/licenses/by-nc-nd/4.0/).

1. Introduction

International safeguards play a crucial role in spreading the peaceful use of nuclear energy across the world. In accordance with the Treaty on the Non-Proliferation of Nuclear Weapons, signatories that are classified as non-nuclear weapons states are required to accept international safeguards if they wish to use nuclear energy. Considering the presence of fissile isotopes (mainly ^{235}U, ^{239}Pu, and ^{241}Pu in civilian nuclear fuel cycles, safeguards are important to ensure these weapons usable materials are not used for nefarious purposes. Current international safeguards are carried out by the International Atomic Energy Agency (IAEA). Although the IAEA is a large organization, resources are limited due to its international scope and global increases in nuclear technology. Removing or minimizing safeguards on non-weapons useable plutonium would allow the IAEA to allocate resources to higher risk materials. This is a key point in analyzing the safeguard limits of plutonium.

When a uranium isotope absorbs a neutron and does not fission, the following decay chain leads to the generation of a plutonium isotope. Thus, any reactor using uranium as its fuel will be producing plutonium. This presents a proliferation risk in every civilian nuclear fuel cycle. Plutonium upon separation can be weaponized due to the presence of ^{239}Pu and ^{241}Pu, both of which are fissile. Depending on the uranium vector in the fresh fuel and the burnup, the plutonium vector in the used fuel could be more or less attractive for weapons purposes.

Increased percentages of ^{238}Pu in used fuel has become a leading candidate for increased proliferation resistance [1,2]. Considering the relatively high alpha decay heat and spontaneous fission rate of ^{238}Pu, elevated percentages of this isotope makes the plutonium vector much less attractive for weapons purposes. Increasing proliferation resistance could also have a major impact on international safeguards. Currently all plutonium is subjected to international safeguards with the exception of plutonium containing greater than 80 at. % ^{238}Pu [3]. Previous research has claimed that a plutonium vector with as low as 18.14 wt. % ^{238}Pu is potentially proliferation-proof [4], however this claim requires more investigation. Decreasing the 80% threshold of ^{238}Pu required

for safeguards exclusion could save valuable resources that can be better applied elsewhere.

Attempting to weaponize a plutonium vector with increased amounts of [238]Pu leads to two major obstacles. An increased decay heat leads to higher temperatures within a hypothetical nuclear explosive device (HNED). If the temperature within the high explosives reaches above the self-explosion temperature, the HNED would be rendered useless. Increase in temperature can also lead to thermal expansion in materials that have positive coefficient of thermal expansion. Once assembled, the components of the HNED are not allowed to freely expand which would lead to thermal stresses within the materials. If the thermal stresses in the materials are above the tensile strengths of the materials, then the materials will fail in the form of ductile failure. Introducing fractures or plastic deformation into the materials will cause the HNED to underperform or fail during the implosion process. Both the temperature profile and thermal stress are dependent on time. Determining the time required to surpass the limits previously mentioned sets a time limit on the usability of the HNED.

2. Materials and methods

2.1. The model geometry and scenarios

The model analyzed in this study represents a spherical implosion type nuclear weapon. This model is considered to be a modernized design due to its minimal plutonium mass (4.9 kg) with a pre detonation k_{eff} of 0.66. Considering smaller plutonium masses create less decay heat, this model represents a limiting scenario. Table 1 shows the radial thickness and material of each spherical shell of the model.

The plutonium is in delta phase with a density of 15.8 g/cm^3. For stability, the plutonium is alloyed with ~5 at. % gallium. Alloying the plutonium with gallium helps prevent phase changes with increasing temperature [6]. The plutonium vector used in this study is shown in Table 2. This plutonium vector is obtained utilizing ORIGEN2 software with a generic 17 × 17 pressurized water reactor static neutron flux profile. The fuel design chosen is Lightbridge's 19.7 wt. % [235]U metallic fuel [7]. This design was selected because the used fuel contains a large isotopic fraction of [238]Pu and is more likely to enter industry use in the near future than other high-burnup fuels. This fuel was simulated with a burnup of 191 MWd/kg. Since the fuel burnup and material composition are outside the validated bounds of ORIGEN2 the exact values shown in Table 2 may not match experimental results. However, this plutonium vector is meant to show that high [238]Pu content plutonium is likely to be produced in the commercial nuclear fuel cycle in the not to distance future and that this plutonium vector can be used to demonstrate the methodology described in this paper.

In order to determine the decay heat produced in this model, the decay heat of each isotope must be known. Table 3 shows the decay heat of each plutonium isotope in units of W/kg. These values are multiplied by the mass of each isotope in the model to calculate the

Table 2
Plutonium vector [4].

Isotope	wt. %
[238]Pu	18.14
[239]Pu	35.66
[240]Pu	21.08
[241]Pu	13.54
[242]Pu	11.58

Table 3
Decay heat [W/kg] [4].

Isotope	α	β
[238]Pu	557.43	–
[239]Pu	1.88	–
[240]Pu	6.94	–
[241]Pu	–	3.22
[242]Pu	0.11	–

total decay heat. The decay heat produced by gamma emission and spontaneous fission are negligible [4]. The total decay heat for this model is 494 W.

This study consists of four unique scenarios in which this model may be used for weapons purposes.

1. In the first scenario, the plutonium pit is inserted into the HNED. The HNED is stationary in a large empty room transferring heat to its surroundings by way of natural convection and radiative heat transfer. Before insertion, the plutonium pit temperature profile reaches steady state and the outer shells of the HNED are at room temperature. The plutonium pit is then inserted allowing for heat transfer by way of heat conduction between the plutonium pit and the outer shells.
2. In the second scenario, the plutonium pit is externally cooled in liquid nitrogen and then inserted into the HNED. The HNED is stationary in a large empty room transferring heat to its surroundings by way of natural convection and radiative heat transfer. The initial temperature of the plutonium in this scenario is the steady state temperature profile while the plutonium pit is in the liquid nitrogen. As with scenario one, once inserted heat will be transferred from the plutonium pit to the outer shell by way of heat conduction.
3. In scenario three, the plutonium pit is inserted into the HNED which is externally cooled with liquid nitrogen. The initial temperature of the plutonium is the same as in scenario one. However, the initial temperature of the outer shells is the temperature of the liquid nitrogen.
4. In scenario four, the fully assembled HNED is initially externally cooled in liquid nitrogen and then removed. The HNED is stationary in a large empty room transferring heat to its surroundings by way of natural convection and radiative heat transfer. The initial temperature profile is the steady state profile when the HNED is externally cooled (scenario 3).

2.2. Determining the temperature profile

The temperature within the HNED is transferred by way of heat conduction. The temperature profile is governed by the transient heat equation as shown in equation (1). Since the temperature only depends on time and radius, the equation is can be simplified from its more complex form. In equation (1), T is the temperature, t is the time, r is the radius, g is the heat generation, k is the thermal conductivity, ρ is the density, and C_p is the heat capacity.

Table 1
Model Geometry [4,5].

Material	Radial Thickness [cm]
Inner cavity	3.715
Pu	1.285
Be	2
U_{dep}	3
PBX 9502	10
Aluminium casing	1

$$\frac{1}{r^2}\frac{1}{\delta r}\left(kr2\frac{\delta T}{\delta r}\right)+\dot{g}=\rho C_p\frac{\delta T}{\delta t} \tag{1}$$

2.2.1. Steady state

Equation (1) must first be solved for the steady state temperature profile (where temperature has no time dependence). This solution is solved for both the plutonium pit (where $\dot{g}$ne;0) and the outer shells (where $\dot{g}=0$). The general solution for the steady state temperature profile within the plutonium pit is shown in equation (2). Equation (2) shows the temperature (T) as a function of radius (r), the inner radius of the shell (r_i), the outer radius of the shell (r_o), the thermal conductivity (k), the heat generation ($\dot{g}$) and the outer temperature of the shell (T_o).

$$T(r)=-\frac{\dot{g}r^2}{6k}-\frac{\dot{g}r_i^3}{3kr}+\frac{\dot{g}r_o^2}{6k}+\frac{\dot{g}r_i^3}{3kr_o}+T_o \tag{2}$$

The solution for the outer shells is shown in equation (3). Equation (3) shows the temperature profile (T) as a function of radius (r), the inner radius of the shell (r_i), the outer radius of the shell (r_o), the thermal conductivity (k), the inner temperature of the shell (T_i), and the outer temperature of the shell (T_o).

$$T(r)=\frac{r_o r_i(T_i-T_o)}{r(r_o-r_i)}-\frac{r_i(T_i-T_o)}{r_o-r_i}+T_o \tag{3}$$

In order to calculate the exact solution for the temperature profile within the HNED, the boundary conditions must be used. At the outermost surface of the HNED, the heat is transferred by way of natural convection and radiation. Equation (4) shows the relationship between the thermal energy transferred at the surface (Q) and the surface temperature (T_s), the temperature of the surroundings (T_{surr}), the temperature of the surrounding wall (T_∞), the surface area (A), the convective heat transfer coefficient (h), the radiative heat transfer coefficient (ε), and the Stefan-Boltzmann constant (σ).

$$\dot{Q}=\varepsilon\sigma A\left(T_s^4-T_{surr}^4\right)+hA(T_s-T_\infty) \tag{4}$$

Since the heat is transferred between the shells by way of heat conduction, the temperature profile is continuous throughout the HNED. Although the assumption of perfect contact between the shells may be slightly unrealistic, this assumption represents a best scenario and will produce lower temperatures than if a slight gap were accounted for. Each shell can be treated as part of a thermal resistance circuit where the outermost temperature is known and the thermal energy transferred through each shell is constant. Equation (5) shows the relationship between the thermal energy ($\dot{Q}$) and the inner radius of the shell (r_i), the outer radius of the shell (r_o), the inner temperature of the shell (T_i), the outer temperature of the shell (T_o), and the thermal conductivity (k).

$$\dot{Q}=\frac{4\pi r_o r_i k(T_i-T_o)}{r_o-r_i} \tag{5}$$

2.2.2. Transient

In order to calculate the transient temperature profile, equation (1) must be discretized. In order to discretize equation (1), the derivate with respect to the radius must be expanded. Equation (6) shows the expanded version of equation (1).

$$\frac{2k}{r}\frac{\delta T}{\delta r}+k\frac{\delta^2 T}{\delta r^2}+\dot{g}=\rho C_p\frac{\delta T}{\delta t} \tag{6}$$

Equations (7)–(9) shows the forward finite difference discretization of the first derivatives (equations (7) and (8)) and a central forward difference discretization of the second radial derivative (equation (9)) [8]. i corresponds to the ith spacial node. j corresponds to the jth time node. Δr is the spacial step size. Δt is the time step size.

$$\frac{\delta T}{\delta r}=\frac{T_{i+1}^j-T_i^j}{\Delta r} \tag{7}$$

$$\frac{\delta T}{\delta t}=\frac{T_i^{j+1}-T_i^j}{\Delta t} \tag{8}$$

$$\frac{\delta^2 T}{\delta r^2}=\frac{T_{i+1}^j-2T_i^j+T_{i-1}^j}{\Delta r^2} \tag{9}$$

Substituting equations (7)–(9) into equation (6) produces equation (10). This equation was solved for the temperature at the $j+1$ time step. Equation (10) was modeled in Matlab.

$$T_i^{j+1}=\frac{k\Delta t}{\rho C_p\Delta r}\left[\frac{2}{r}\left(T_{i+1}^j-T_i^j\right)+\frac{1}{\Delta r}\left(T_{i+1}^j-2T_i^j+T_{i-1}^j\right)\right]+T_i^j+\frac{\dot{g}\Delta t}{\rho C_p} \tag{10}$$

The only stability criteria for equation (10) is shown in equation (11).

$$\frac{k\Delta t}{\rho C_p\Delta r^2}<\frac{1}{2} \tag{11}$$

The boundary conditions for the transient temperature profile is similar to those of the steady state. The temperature profile is continuous within the HNED. At the outermost surface of the HNED, the same convective and radiative heat transfer boundary condition described in equation (4) applies. This boundary condition is shown in equation (12).

$$\frac{\delta T}{\delta r}=\varepsilon\sigma\left(T_s^4-T_{surr}^4\right)+h(T_s-T_\infty) \tag{12}$$

Fourier's law (shown in equation (13)) applies at each interface. In equation (13), k_m is the thermal conductivity of the mth shell, k_n is the thermal conductivity of the nth shell, T_m is the temperature profile within the mth shell, T_n is the temperature profile within the nth shell, and r_{int} is the radius at the interface.

$$k_m\frac{\delta T_m}{\delta r}\bigg|_{r_{int}}=k_n\frac{\delta T_n}{\delta r}\bigg|_{r_{int}} \tag{13}$$

Equations (12) and (13) can be utilized at each boundary by modifying the finite difference scheme described in equation (10) to reflect the boundary conditions.

2.2.3. Material properties and constants

Table 4 shows the material properties used in this study.

Table 5 shows the convective heat transfer coefficients used in the four scenarios. In order to be conservative, the radiative heat transfer coefficient was chosen to be that of a black body. This is a limiting scenario producing lower temperatures than that of a more realistic scenario.

2.3. Calculating maximum stress

As the temperature within the HNED increases, the shells will expand as it has positive coefficient of thermal expansion. Once assembled, each shell is fixed together without a gap and not

Table 4
Material Properties * [10] ** [11] †[12] ' [13].

Material	Thermal Conductivity [9] [W/m·K]	Density [9] [g/cm^3]	Heat Capacity [9] [J/g·K]
Pu	10.97*	15.8	0.13
Be	102	1.85	1.78
U$_{dep}$	28.9	18.9	0.1163
PBX 9502	0.560656**	1.90**	1.125'
Al casing	98†	2.7	1.177

Table 5
Convective heat transfer coefficients [W/cm^2·K] †[12]‡ [14].

Fluid	Convective Heat Transfer Coefficient
Air	0.001†
Liquid Nitrogen	0.01‡

allowed to expand. This produces thermal stresses within the material. In this study, the thermal stress is considered to be linear due to the fact that the temperature gradient is only in the radial direction. Equation (14) shows the relationship between thermal stress (σ_T), Young's Modulus of Elasticity (E), the temperature difference (ΔT), and the linear thermal expansion coefficient (α).

$$\sigma_T = E \cdot \Delta T \cdot \alpha \qquad (14)$$

If the thermal stress calculated using equation (14) is greater than the tensile strength of the material, then the material will fail by fracture or plastic deformation. The slightest failure within the HNED will likely cause a nonuniform implosion upon detonation of the high explosives. In order to achieve the proper yield, the plutonium must be imploded as uniformly as possible. A nonuniform implosion will result in little to no yield from the HNED effectively reducing its impact to that of a radiological dispersal device.

Table 6 shows Young's Moduli of Elasticity, the linear expansion coefficients, and the tensile strengths used in this study.

3. Results

3.1. Temperature profiles

3.1.1. Scenario 1
Fig. 1 shows the temperature profile at various times within the HNED in scenario 1.

3.1.2. Scenario 2
Fig. 2 shows the temperature profile at various times within the HNED in scenario 2.

3.1.3. Scenario 3
Fig. 3 shows the temperature profile at various times within the HNED in scenario 3.
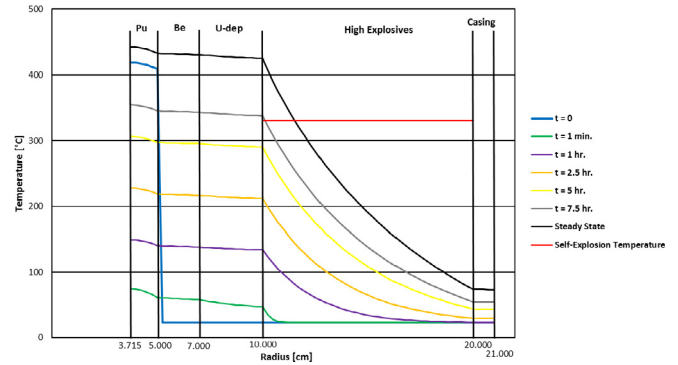

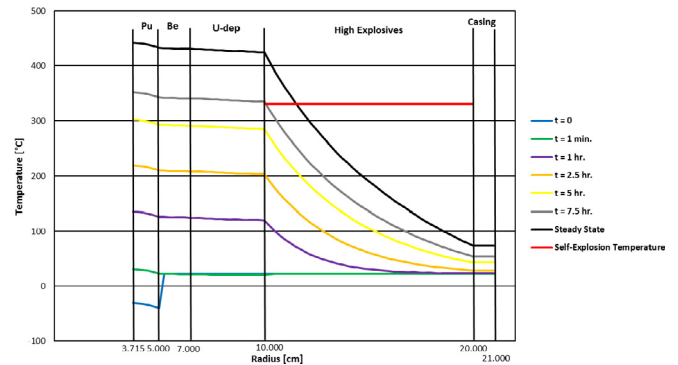**Fig. 1.** Temperature profiles of scenario 1.

Fig. 2. Temperature profiles of scenario 2.

3.1.4. Scenario 4
Fig. 4 shows the temperature profiles at various times within the HNED in scenario 4.

3.2. Maximum thermal stress

Figs. 5–9 show maximum thermal stresses in each material as a function of time. These Figures do not represent the true stress the material would experience over time. Once the tensile strength is surpassed, the material would fail leading to rapid reduction in stresses. These Figures simply show whether or not the thermal stress reaches the tensile strength causing material failure.
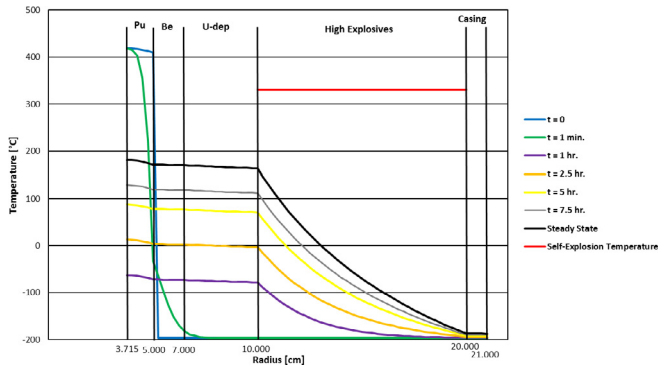
Table 6
Stress Related Material Properties [9,10,15–19].

Material	Modulus of Elasticity [GPa]	Thermal Expansion [1/K]	Tensile Strength [GPa]
Pu	68	3.00E-06	1.00E-01
Be	303	1.60E-05	1.90E-01
U$_{dep}$	190	1.39E-05	6.15E-01
PBX 9502	15.3	4.01E-06	3.23E-03
Al casing	17	2.30E-05	4.80E-01

Fig. 3. Temperature profiles of scenario 3.
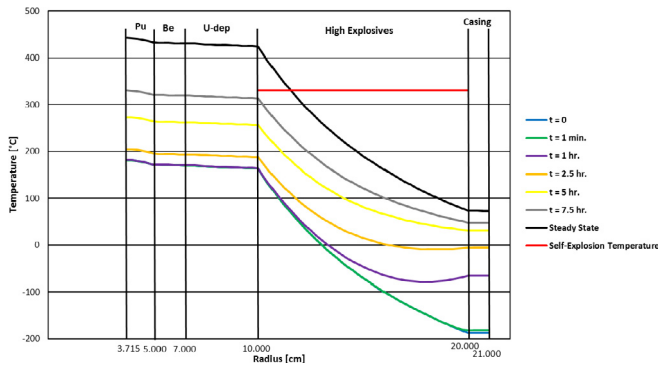

Fig. 4. Temperature profiles of scenario 4.

4. Discussion

4.1. Temperature profiles

The temperature profiles of scenarios 1, 2 and 4 show that the temperature within the high explosives would reach the self-explosion temperature causing the HNED to be rendered useless. The temperature within the high explosives in scenarios 1, 2 and 4 reach the self-explosion temperature in approximately 7.5−8 h, rendering the HNED useless. This fairly short time further bolsters the proliferation resistance of this plutonium vector. In scenario 3, the temperature within the high explosives is well below the self-explosion temperature. However, externally cooling the entire HNED in liquid nitrogen would be a difficult task, likely requiring advanced technology and knowledge. Even in the scenario of external cooling, the HNED would be useless 8 h after the HNED is removed from the cooling, as shown in scenario 4.

4.2. Stresses

Figs. 5−9 show the maximum thermal stress surpasses the tensile strength in several materials. In all four scenarios, the maximum thermal stress in the high explosives and beryllium surpasses the tensile strength, thus causing failure of the HNED in all scenarios. In scenarios 1, 2, and 4, the maximum thermal stress in the uranium surpasses the tensile strength.

In scenarios 1 and 2, the maximum thermal stress in the beryllium surpasses the tensile strength after only a few minutes, thus the HNED would fail after only a few minutes. The HNED would be practically useless in this scenario because delivering it within only a few minutes of insertion would be impractical. This is a much faster timeline than that established by the temperature profiles of the two scenarios which limited the functionality of the HNED to 7.5 h.

In scenario 3, the maximum thermal stress in the beryllium surpasses its tensile strength after 5 h and the maximum thermal stress in the high explosives surpasses its tensile strength after 6 h. Therefor the HNED would fail after about 5 h. This time limit is especially import considering the temperature profile of scenario 3 will not lead to self-explosion. Considering the maximum thermal stress in the beryllium and high explosives are well above the tensile strength of the materials at the steady state of scenario 3, the HNED is not functional at any point in scenario 4.

The results of this study show that for the given plutonium vector of 18.14 wt. % ^{238}Pu, all four time dependent scenarios
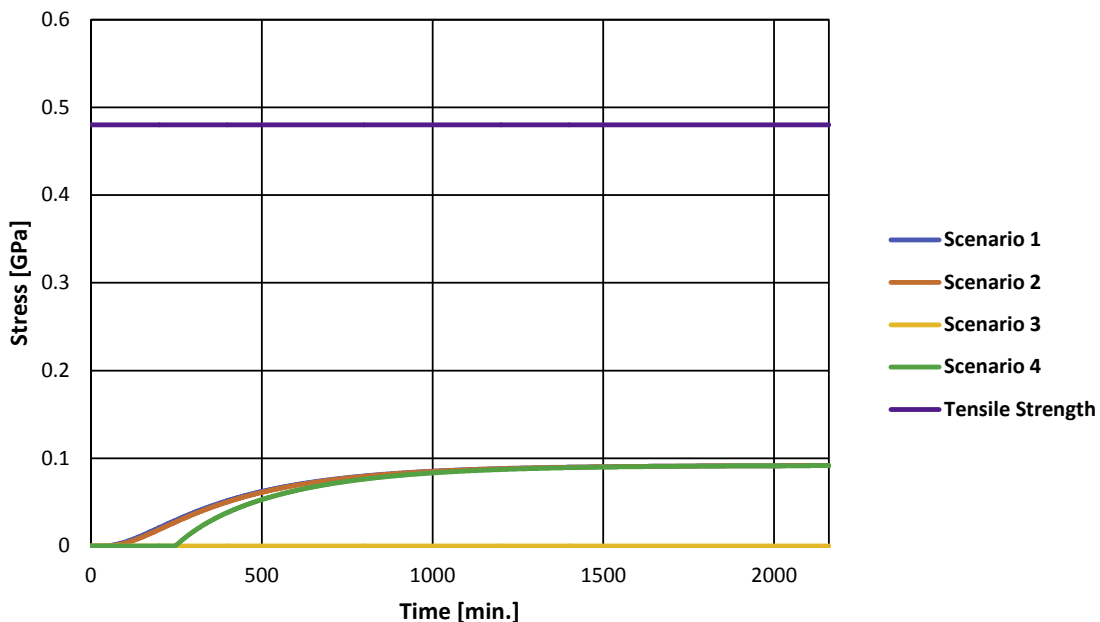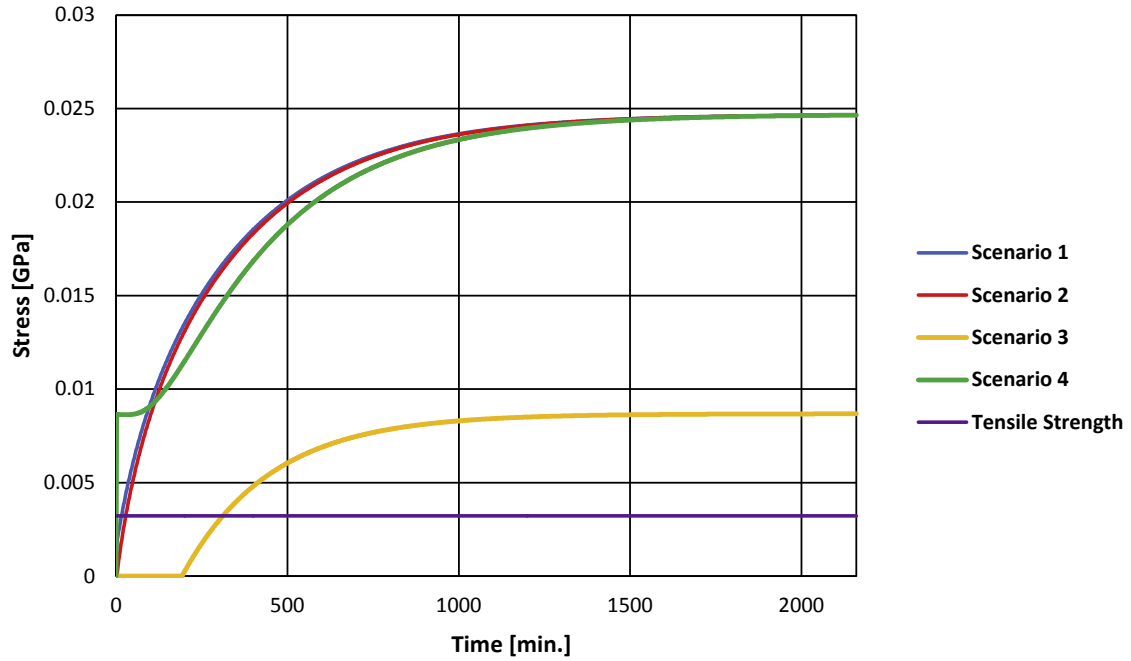

Fig. 5. Maximum stress in the aluminum.

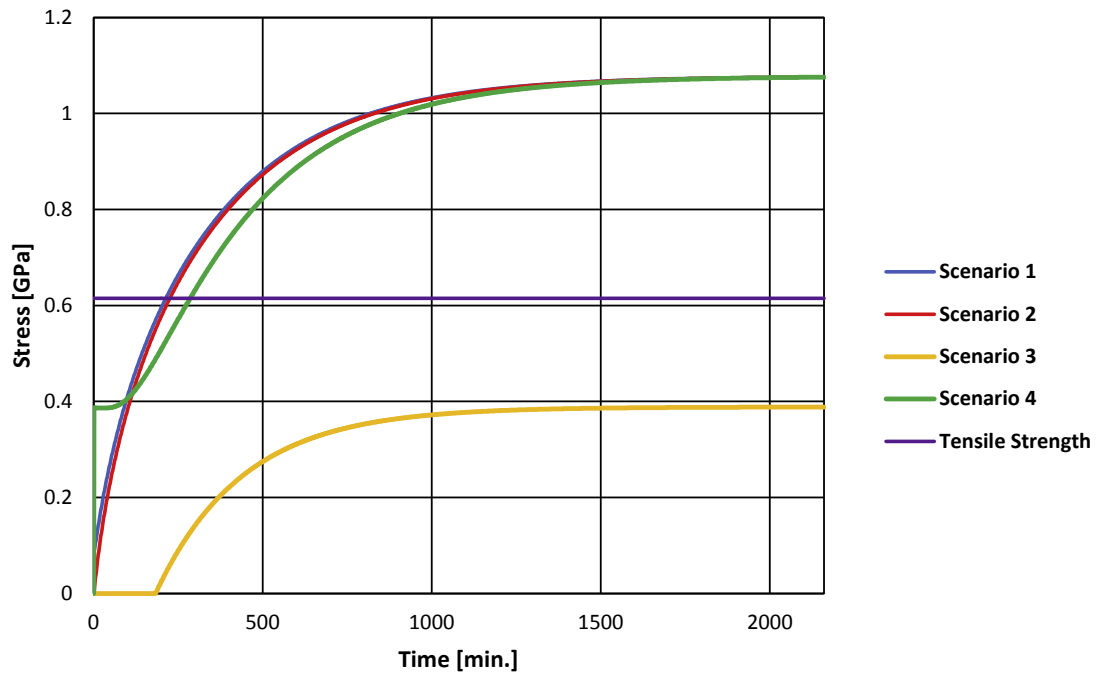**Fig. 6.** Maximum stress in the high explosives.

Fig. 7. Maximum stress in the uranium.

analyzed result in a nonfunctional HNED within a few minutes to 5 h. In addition to this, several of the scenarios require advanced technology and knowledge which may not be available to non-state actors. These results strengthen the argument that high-burnup plutonium could have reduced, and possibly even no, safeguards applied to them. This would allow for the limited safeguards resources to be applied to other more weapons useable materials.

4.3. Evaluation of proliferation resistance

Proliferation resistance has long been a topic of discussion within the safeguards community. However defining proliferation resistance may be difficult. Prior work has been done to define proliferation resistance as it applies to proliferation by state entities [20]. Studies done by Bathke et al. using this definition have developed a Figure of Merit (FOM) that seeks to measure the
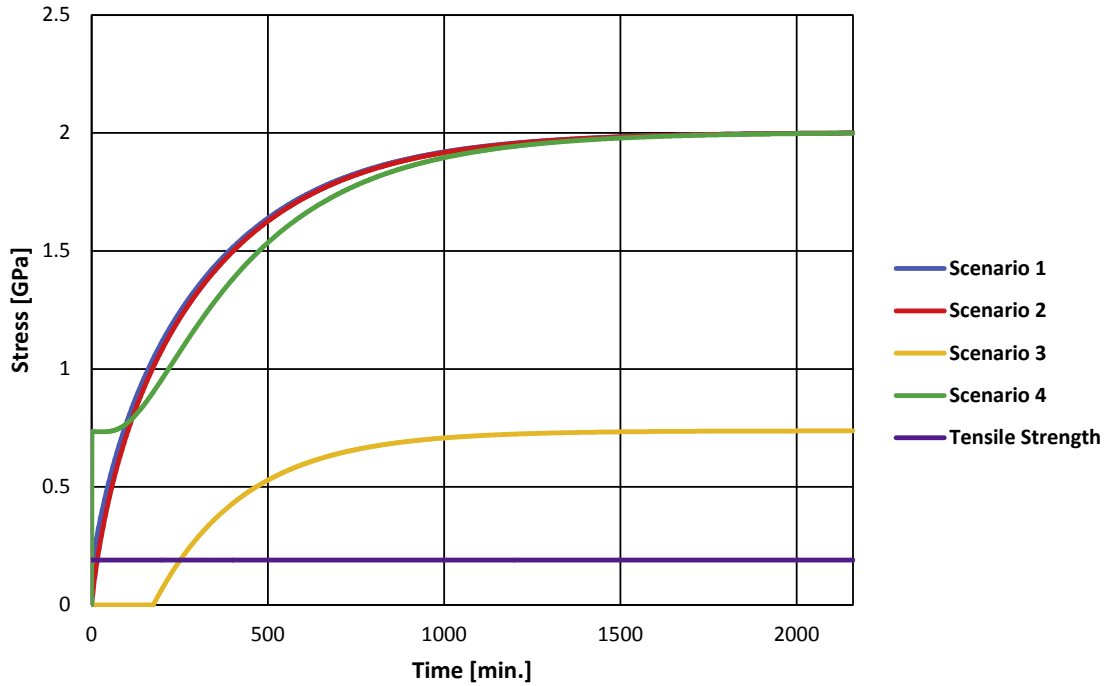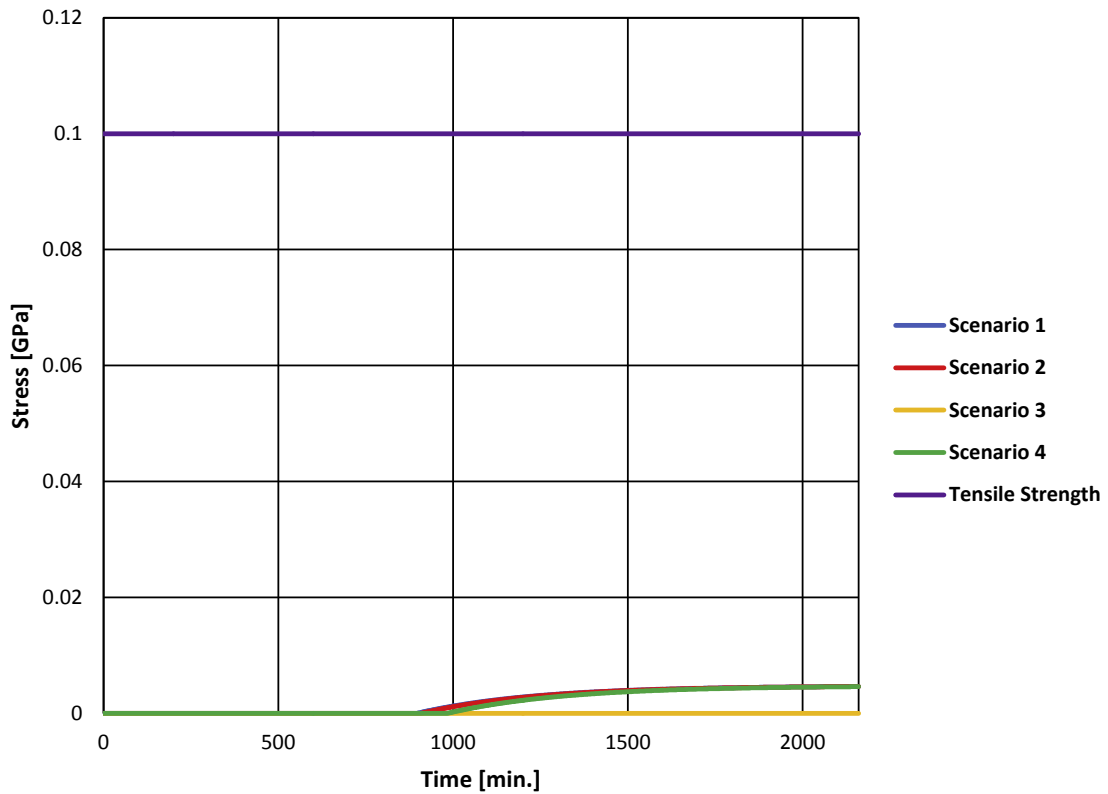
Fig. 8. Maximum stress in the beryllium.

Fig. 9. Maximum stress in the plutonium.

attractiveness of materials as they relate to proliferation by state entities [21]. Considering this FOM was developed using currently agreed upon safeguards limits (such as 80% ^{238}Pu), the plutonium vector used in this study falls well short of being unattractive. However, this study serves as a challenge of the current safeguards limit of 80% ^{238}Pu by evaluating a simple HNED design. Although the technological capabilities of many country surpass the design found here, the results serve as an initial step in evaluating this particular safeguards limit. A comprehensive study of proliferation resistance assessment methodology since 2008 can be found in the

thesis of L. Pierpoint [22].

Acknowledgements

References

[1] Y. Kimura, S. Masaki, H. Sagara, Evaluation of proliferation resistance of plutonium based on decay heat, J. Nucl. Sci. Technol. 48 (5) (2011) 715–723.

[2] G. Kessler, Proliferation-proof Uranium/Plutonium Fuel Cycles, Safeguards and Non-proliferation, first ed., KIT Scientific Publishing, Karlsruhe, 2011.

[3] IAEA, Information Circular, INFCIRC/ 153, 1972.

[4] C. Lloyd, B. Goddard, Proliferation resistant plutonium: an updated analysis, Nucl. Eng. Des. 330 (2018) 297–302.

[5] S. Fetter, V.A. Frolov, M. Miller, R. Mozley, O.F. Prilutsky, S.N. Rodionov, R.Z. Sagdeev, Detecting Nuclear Warheads, Sci. Global Secur. 1 (1990) 225–302.

[6] J.N. Mitchell, M. Stan, D.S. Schwartz, C.J. Boehlert, Phase stability and phase transformations in plutonium and plutonium-gallium alloys, Metall. Mater. Trans. 35A (2004) 2267–2278.

[7] J. Malone, A. Totemeier, N. Shapiro, S. Vaidyanathan, Lightbridge corporation's advanced metallic fuel for light water reactors, Nucl. Technol. 180 (3) (2012) 437–442.

[8] S.C. Chapra, R.P. Canale, Numerical Methods for Engineers, 7 ed., McGraw-Hill, New York, 2015.

[9] IAEA, Thermophysical Properties of Materials for Nuclear Engineering, A Tutorial and Collection of Data, Vienna, 2008.

[10] S.S. Hecker, Plutonium and its Alloys: from Atoms to Microstructure, 2000.

[11] G. Kessler, Plutonium denaturing by ^{238}Pu, Nucl. Sci. Eng. 155 (2007) 53–73.

[12] Y.A. Çengel, Heat Transfer: a Practical Approach, second ed., McGraw-Hill, New York, NY, 2003.

[13] R.K. Weese, A.K. Burnham, H.C. Turner, T.D. Tran, Exploring the physical, chemical and thermal characteristics of a new potentially insensitive high explosive RX-55-AE-5, J. Therm. Anal. Calorim. 89 (2) (2007) 465–473.

[14] M.W. Biddulph, R.P. Burford, Thermal properties and heat transfer coefficients in cryogenic cooling, Cryogenics 22 (6) (1982) 283–286.

[15] A. Goldberg, Atomic, Crystal, Elastic, Thermal, Nuclear, and Other Properties of Beryllium, UCRL-TR-224850, 2006. LLNL.

[16] J.M. Gere, B.J. Goodno, Mechanics of Materials SI, Cengage Learning, Stanford, CT, 2012.

[17] B. Banerjee, D.O. Adams, On predicting the effective elastic properties of polymer bonded explosives using recursive cell method, Int. J. Solid Struct. 41 (2) (2004) 481–509.

[18] S.J.P. Palmer, J.E. Field, J.M. Huntley, Deformation, strengths, and strains to failure of polymer bonded explosives, Proc. of the Roy. Soc. A 440 (1909) 1993.

[19] D.G. Thompson, G.W. Brown, R. Deluca, A.M. Giambra, M.M. Sandstrom, Thermal expansion of PBX 9501 and PBX 9502 plastic-bonded explosives, LA-UR-09-05002, 37th meet. Of the nor, Amer. The. Ana. Soc. September 21 (2009) (Lubbock, TX).

[20] The Proliferation Resistance and Physical Protection Evaluation Methodology Working Group of the Generation IV International Forum. Evaluation Methodology for Proliferation Resistance and Physical Protection of Generation IV Nuclear Energy Systems.

[21] C.G. Bathke, B.B. Ebbinghaus, B.A. Collins, B.W. Sleaford, K.R. Hase, M. Robel, R.K. Wallace, K.S. Bradley, J.R. Ireland, G.D. Jarvinen, M.W. Johnson, A.W. Prichard, B.W. Smitj, The attractiveness of materials in advanced nuclear fuel cycles for various proliferation and theft scenarios, Nucl. Technol. 179 (1) (2017) 5–30.

[22] L.M. Pierpoint, Analyzing the Proliferation Resistance of Advanced Nuclear Fuel Cycles: in Search of an Assessment Method for Use in Fuel Cycle Simulations, Thesis, Massachusetts Institute of Technology, Feb. 2008.